ACS APPLIED MATERIALS & INTERFACES

Research Article

www.acsami.org

Highly Efficient and Recyclable Nanocomplexed Photocatalysts of AgBr/N-Doped and Amine-Functionalized Reduced Graphene Oxide

Md. Selim Arif Sher Shah,[†] Woo-Jae Kim,[‡] Juhyun Park,[§] Do Kyung Rhee,[†] In-Hyuk Jang,[†] Nam-Gyu Park,[†] Jun Young Lee,[†] and Pil J. Yoo*[,†,∥]

[†]School of Chemical Engineering, Sungkyunkwan University, Suwon 440-746, Republic of Korea

[‡]Department of Chemical and Environmental Engineering, Gachon University, Songnam 461-701, Republic of Korea

[§]School of Chemical Engineering and Materials Science, Chung-Ang University, Seoul 156-756, Republic of Korea

[∥]SKKU Advanced Institute of Nanotechnology (SAINT), Sungkyunkwan University, Suwon 440-746, Republic of Korea

Supporting Information

ABSTRACT: Although silver bromide has recently drawn considerable attention because of its high photocatalytic activity, it tends to form agglomerated metallic silver under the irradiation of visible light. Therefore, photocatalytic activity decreases with time and cannot be applied for repeated uses. To overcome this limitation, in the present work, we complexed AgBr with nitrogen doped (N-doped) and amine functionalized reduced graphene oxide (GN). N-doped and/or amine functionalized graphene shows intrinsically good catalytic activity. Besides, amine groups can undergo complexation with silver ions to suppress its reduction to metallic Ag. As a result, these complexed catalysts show excellent photocatalytic activity for the degradation of methylene blue (MB) dye under the irradiation of visible light. Photocatalytic degradation of MB shows that the catalytic activity is optimized at a condition of 0.5 wt % GN, under which ~99% of MB was degraded only after 50 min of visible light irradiation. Notably, the complexed catalyst is quite stable and retained almost all of its catalytic activity even after greater than 10 repeated cycles. Moreover, the catalyst can also efficiently decompose 2-chlorophenol, a colorless organic contaminant, under visible light exposure. Detailed experimental investigation reveals that hydroxyl (·OH) radicals play an important role for dye degradation reactions. A relevant mechanism for dye degradation has also been proposed.

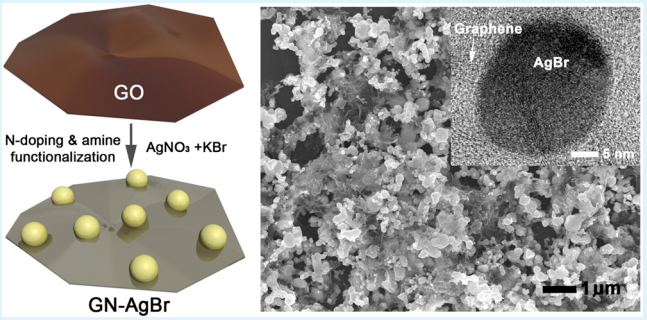

KEYWORDS: *photocatalyst, amine functionalized graphene, N-doping, AgBr, stability, recyclability*

INTRODUCTION

In recent years, a great deal of attention has been paid to solve the problem of widespread pollution caused by organic pollutants.[1,2] For example, most organic dyes, released from textile industries, are highly toxic and nonbiodegradable. Photolysis of these dyes creates secondary pollution; thus, they are the main source of environmental contamination.[2,3] In this regard, photodegradation of organic pollutants, especially under visible light, is more accessible than other available processes, such as physical, chemical, or biological methods.[3−8] A number of semiconductor based photocatalysts have been utilized as photoactive materials to degrade the pollutants. For example, TiO_2 is well utilized because of its abundance and relative low toxicity, whereas its photocatalytic function is only limited under UV irradiated conditions because of its bandgap located in the UV region.[3,9,10] Therefore, the necessity of visible light driven photocatalyst has been continuously raised. Among different visible light driven photocatalysts, silver halides, especially AgBr, found their important place to the research communities, primarily because of its good sensitivity to visible light and high photocatalytic activity. Despite its notable advantages, AgBr photocatalyst confronts an intrinsic limitation of its instability because it is highly susceptible to reduction to metallic Ag under the irradiation of light.[1,2,4−11]

In general, to facilitate the photocatalytic activity, together with an increased surface area, AgBr is loaded on the support of other materials. However, those composite materials can rarely exploit the full catalytic activity of AgBr.[12,13] For example, Zang et al. reported a composite catalyst of Y-zeolite and AgBr as a highly active photocatalyst under visible light.[14] However, the catalyst has failed to achieve the stability for long time use. Recently, as an improved system, plasmonic photocatalysts of Ag@AgBr were reported by several groups.[15−17] These catalysts show much enhanced photocatalytic activity under visible light due to the synergistic incorporation of the localized surface plasmon resonance (LSPR) effect of Ag nanoparticles, which are intimately located on the surface of the active catalyst. However, in most cases, the synthetic schemes consist

Received: August 1, 2014
Accepted: November 11, 2014
Published: November 11, 2014

of multisteps and therefore are highly time-consuming. Moreover, the synthesized Ag nanoparticles are undesirably large and polydispersed in their sizes. Those aspects eventually result in a serious drawback in the catalytic activity because the LSPR effect strongly depends on the shape, size, and distribution of Ag nanoparticles.[18−20] It has been also reported for a template-free synthesis of Ag/AgCl nanocubes and their highly efficient photocatalytic activity.[21] However, the repeatability of the catalysts has not been properly investigated as well.

Recently graphene, a single atom thick and sp^2 hybridized carbon atoms, drew extensive attention for its outstanding physical and chemical properties and great promise in the fields of electronics and materials science.[22−35] In the field of photocatalytic applications, for example, Liu et al. demonstrated ternary nanocomposite of Ag/AgBr/graphene oxide synthesized through oil-in-water and water-in-oil microemulsion technique.[22] The catalyst showed high photocatalytic activity under sunlight irradiation. The catalytic activity, however, still markedly decayed over repeated uses. Moreover, in this approach, the graphene oxide was used as a simple structural support, not as a conductive matrix like graphene or reduced graphene oxide. On the basis of this background, it is necessary and timely to develop a novel photocatalyst for visible light irradiation, which is structurally and functionally stable even after prolonged use.

Although the chemically reduced graphene oxide has been extensively exploited for synthesizing nanocomposite photocatalysts, it has the natural tendency to stack and undergo irreversible aggregation which gradually mitigates the properties of graphene.[36] To challenge this problem, it is possible to enhance the physicochemical properties of graphene by chemical modification and/or doping with heteroatoms.[37,38] Nitrogen doped graphene shows substantially enhanced catalytic and electronic properties.[39−41] In particular, amine functionalized graphene has recently been shown to have enhanced catalytic activity toward oxygen reduction reaction and the amino groups are observed to impart extra stability to the catalyst.[38,42] Moreover, amine groups can readily go through complexation with Ag^+ ions and bind them closely and tightly.[43] In this way amine groups suppress the formation of self-reduced metallic Ag.[1,43]

Therefore, in the present work, nanocomposites of AgBr with reduced graphene oxide, which is both amine functionalized and nitrogen doped (hereafter, it will be termed GN), were for the first time synthesized and their outstanding photocatalytic effect was examined for repeated uses. Notably, it is expected that high conductivity of GN can disperse the photogenerated electrons far away from AgBr as soon as they are generated. Hence, the undesirable degradation of AgBr through the spontaneous reduction to metallic Ag is expected to be reduced greatly. Moreover, synthetic process to prepare the composites of AgBr and GN was facile and carried out under mild conditions of ambient temperature and pressure, without using harsh and toxic chemicals. Therefore, it is anticipated that this catalyst and synthetic approach will be suitable to be followed in industry to remove organic pollutants or toxic chemicals.

EXPERIMENTAL SECTION

Materials. Graphite, silver nitrate, potassium bromide, and methylene blue were purchased from Sigma-Aldrich. Potassium permanganate, hydrogen peroxide, and ethanol were purchased from Sinopharm Pvt. Ltd. All the chemicals were used as received without further purification. Deionized (DI) water with a resistance of 18.2 MΩ was used as the solvent. Graphene oxide (GO) was synthesized using a modified Hummers method which is described elsewhere.[10]

Synthesis of N-Doped and Amine Functionalized Reduced Graphene Oxide. Amine functionalized graphene was synthesized following a reported method with some modifications.[32] In short, 100 mg of GO powder was dispersed in 31 mL of deionized water by sonication for several hours. Then ascorbic acid of 0.9 g was dissolved in the dispersion. Ammonium hydroxide of 1.5 mL was added, and the mixture was transferred to a 50 mL Teflon liner. It was then autoclaved at 180 °C for 12 h. The resultant product of both N-doped and amine functionalized reduced graphene oxide (GN) was finally collected after washing with copious amount of DI water. Reduced graphene oxide, rGO, was synthesized in the same way without adding NH_3 solution.

Synthesis of AgBr@GN. In a typical experiment, depending on the composition of the catalyst, a known amount of amine functionalized graphene oxide was dispersed in 20 mL of ethanol by sonication for hours. A solution of 1.40 mmol of $AgNO_3$ in 40 mL of water was added to GN dispersion under vigorous stirring. Gentle stirring was continued for 4 h at room temperature. A solution of 1.70 mmol of KBr in 20 mL water was added dropwise under vigorous stirring. Stirring was further continued at ambient temperature for 12 h. The obtained black precipitate was washed with DI water to remove excess KBr and dried at 60 °C overnight. The overall synthetic procedure is summarized in Scheme 1. In the same way, composite of rGO with AgBr was synthesized. Hereafter, the composites will be designated as *x*GN/rGO−AgBr, where *x* is the weight percentage of GN/rGO in the composite. AgBr was also prepared following the same recipe without inclusion of graphene oxide. A mixture of amine functionalized reduced graphene oxide and as prepared AgBr was prepared by physical mixing, and its photocatalytic activity was compared with that of the other catalysts. It is designated as *x*GN−AgBr mix, where the meaning of *x* is the same as previous one. For comparison nitrogen doped titania (denoted as N−TiO_2) was prepared following a reported method.[44]

Scheme 1. Procedure for Synthesizing the GN−AgBr Nanocomposites

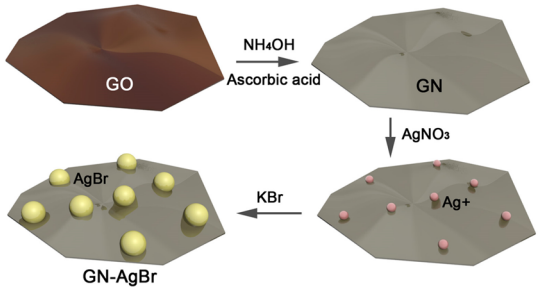

Degradation of Methylene Blue. In a typical experiment, 30 mg of catalyst was dispersed in a solution of 0.8 mL of methylene blue (0.6 mM) in 39.2 mL of DI water. The mixture was sonicated in a bath sonicator (Power Sonic 420) for 2 min and then stirred under darkness for 1 h to establish adsorption−desorption equilibrium between the dye and the catalyst. It was then exposed to a solar simulator (Ls-150-Xe lamp, Abet Technologies, USA) equipped with a 150 W Xe arc lamp, radiating visible light (>400 nm) while maintaining a distance of 10 cm from the source. Approximately 4 mL of the reaction mixture was taken out in a regular interval. The concentration of the dye was determined by measuring its absorbance with a UV−visible spectrophotometer. 2-Chlorophenol was analyzed with a high performance liquid chromatography (HPLC) (1100 HPLC System, Agilent Technologies) instrument. Two mobile phases, (i) 0.1% formic acid in water and (ii) 0.1% formic acid in acetonitrile, were used. Other experimental conditions for HPLC are the following: column, Agilent Poroshell 300 SB-C18, 2.1 mm × 100 mm, 2.7 μm; flow rate of 0.2 mL/min; detection, UV 280 nm; injection, 10 μL.

Photocurrent Measurements. Working electrodes were prepared in the following way. At first, a slurry was prepared by mixing 20 mg of the catalyst with 40 mg of ethyl cellulose (Sigma-Aldrich) and 100 μL of α-terpineol (Sigma-Aldrich). The slurry was then spread over 1 × 2 cm^2 area on the conducting side of ITO glass. Ethyl cellulose and α-terpineol were removed by heating the ITO at 300 °C for 30 min as described in our previous work.[9] Photoelectrochemical measurement was carried out in a three-electrode system, where the catalyst film was acting as working electrode, a Pt foil acts as a counter electrode, and Ag−AgCl electrode acts as a reference electrode. An aqueous solution of 0.5 M Na_2SO_4 was used as electrolyte. In this experiment a portable solar simulator (PEC-L01, Piccell, IRIE Corporation, Japan) was used as the visible light source and a potential of 0.6 V was applied. The photocurrent was measured with an electrochemical analyzer (CHI608C, CH Instruments, Austin, TX).

Characterization. Powder X-ray diffraction (XRD) patterns were obtained (D8 Focus, Bruker, Germany) with Cu Kα radiation (λ = 1.5406 Å) in the 2θ range from 2° to 80° with a scan rate of 3 deg min^{-1}. The accelerating voltage and the applied current were 40 kV and 40 mA, respectively. Transmission electron microscopy was carried out with a TECNAI G2 instrument with an acceleration voltage of 300 kV. FTIR measurements (IFS-66/S, Bruker, Germany) were carried out in the transmittance mode in the spectral range of 400−4000 cm^{-1} with a resolution greater than 0.1 cm^{-1}. UV−visible absorption and diffuse reflectance spectra (DRS) were collected from the UV−vis−NIR spectrophotometer (UV-3600, Shimadzu, Japan). Raman spectra were taken using a micro-Raman spectrometer system (ALPHA 300M, WITec, Germany). The sample was loaded on silica wafer and focused using a 50× objectives. The spectra were taken in the range of 1−3000 cm^{-1}. X-ray photoelectron spectroscopy (XPS) characterization was performed (ESCA 2000 instrument, VG Microtech, U.K.) with Al Kα X-ray source. All the binding energy values were corrected with a calibration of the C 1s peak at 284.6 eV. High resolution peaks were deconvoluted using Gaussian−Lorentzian functions with identical full width at half maxima (fwhm) after a Shirly background subtraction. Photoluminescence data were collected in a Cary Eclipse fluorescence spectrophotometer (Agilent Technologies). The Brunauer−Emmett−Teller (BET) specific surface areas and porosity of the samples were evaluated on the basis of nitrogen adsorption isotherms measured at −196 °C using a gas adsorption apparatus (ASAP 2020, Micromeritics, USA).

RESULTS AND DISCUSSION

Powder X-ray diffraction (PXRD) was used to analyze the phase of the synthesized materials. PXRD of GN, as depicted in Figure 1A, shows a broad peak at 2θ, ~25.3°, and absence of any peak at ~12°. These two observations prove the successful reduction of GO to GN.[9,10] PXRD pattern of AgBr can be indexed to face centered cubic (fcc) crystal of AgBr (JCPDS card no. 6-438).[45] Comparison of PXRD pattern of AgBr with that of the composite 1GN−AgBr reveals that these two diffraction patterns are essentially identical as evident from Figure 1A. No other peaks for impurities or other phases like Ag or Ag_xO were observed, implying that the composite consists of pure AgBr. It should be noted that the XRD of the composite does not show any specific peak for GN. It is due to the relatively small amount of GN in the composite (1 wt %) and strong intensity of the AgBr peaks to suppress the emergence of GN peaks. At this point, it is necessary to mention that the PXRD pattern, shown in Figure S1 in Supporting Information, of the composite catalyst after 11 catalytic cycles shows a weak peak at 2θ, 38.1°, which is due to the metallic Ag, produced by the reduction of small amount of AgBr during repeated photocatalytic experiments.[46] Further evidence in support of this explanation will be discussed in XPS data analysis.

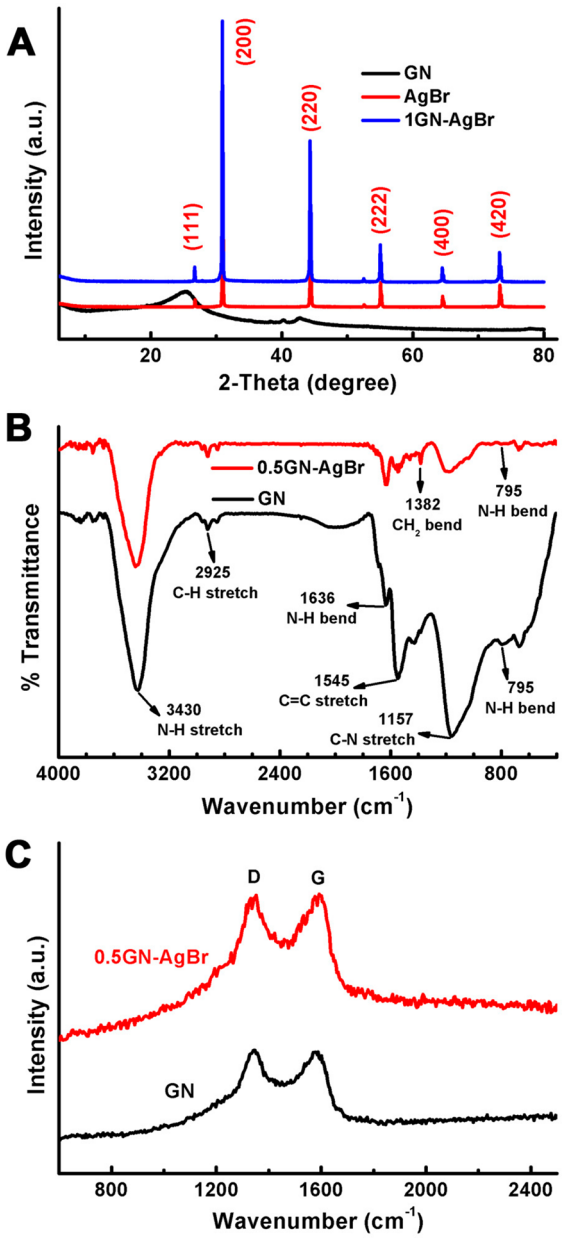

Figure 1. Crystallographic and chemical characterizations of the synthesized complexes. (A) Powder X-ray diffractograms of GN, AgBr, and 1GN−AgBr. (B) FTIR and (C) Raman spectra of GN and the composite 0.5GN−AgBr.

Figure 1B shows the FTIR spectra of GN and the composite 0.5GN−AgBr. In GN, N−H bending vibration of amine groups appears at 1636 and 795 cm^{-1}.[38] Aromatic C=C stretching frequency shows a peak at 1545 cm^{-1}.[9,10] The broad peak at ~3430 cm^{-1} can be ascribed to N−H and O−H stretching vibrations. The FTIR spectrum of 0.5GN−AgBr is almost the same as that of GN. While the N−H bending in GN appears at 1636 cm^{-1}, this peak has slightly shifted to a lower value, 1630 cm^{-1}, in the composites. It is presumably due to the complexation of Ag^+ ions in AgBr to the amine functional groups of GN.[43] However, such an interaction is less pronounced for the peak at 3430 cm^{-1} because of its broadness. CH_2 bending in 0.5GN−AgBr appears at ~1382 cm^{-1}. As delineated in Figure 1C, Raman spectrum of GN shows the presence of D and G bands at 1344 and 1583 cm^{-1}.[9,10] On the

dx.doi.org/10.1021/am5051422 | ACS Appl. Mater. Interfaces 2014, 6, 20819−20827

other hand, the composite of 0.5GN−AgBr shows these bands to be present at 1349 and 1594 cm^{-1}, respectively. The shifting of the D and G bands in the composite compared to GN indicates the occurrence of interactions between AgBr and the amine functionalized reduced graphene oxide. The I_D/I_G (ratio of intensity of D band to G band) values of GN and 0.5GN−AgBr are respectively 1.05 and 1.06. The increased value of I_D/I_G in 0.5GN−AgBr is due to the creation of more defects in it after the attachment of AgBr with GN.

Figure 2A and Figure 2B depict typical SEM micrographs of 0.5GN−AgBr. It is obvious from the SEM micrograph that the AgBr nanoparticles are well covered and layered with GN nanosheets. The AgBr nanoparticles exist in different shapes and sizes. SEM micrograph of the used catalyst of 0.5GN−AgBr is shown in Figure S2, which represents little difference between before and after use of the catalysts. Figure 2C shows the TEM micrograph of 0.5GN−AgBr. Figure S3 depicts TEM micrograph of 2GN−AgBr for increased amount of GN. These micrographs clearly exhibit that AgBr nanoparticles are nearly uniformly distributed over GN. To observe the crystallized structure more precisely, high resolution TEM (HRTEM) micrograph of 0.5GN−AgBr is presented in Figure 2D. The fringe lines reveal that the interspacing is 2.88 Å, which is indicative of (200) planes of AgBr nanocrystals.[47]

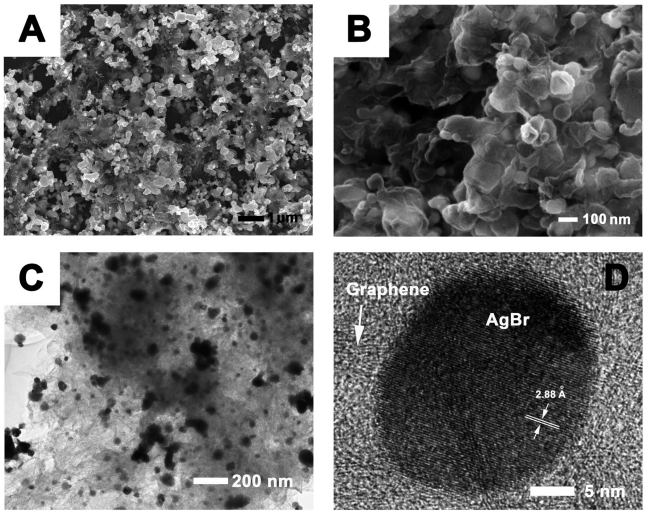

Figure 2. Microscopic observation for synthesized catalysts. Parts A and B are SEM micrographs of 0.5GN−AgBr. Part C is the TEM micrograph of 0.5GN−AgBr, and part D is its HRTEM image.

Compositions and chemical state of the synthesized materials were examined by X-ray photoelectron spectroscopy (XPS). High resolution XPS spectrum of nitrogen in GN, presented in Figure 3A, shows different types of N atoms. The peaks at 398.81 (2.59 atom %), 400.11 (5.34 atom %), and 401.73 (0.82 atom %) eV are designated as amino, pyrrolic, and graphitic N, respectively.[29,32] The as synthesized GN contains atomic concentrations of C, O, and N with percentages of 81.1, 10.1, and 8.8, respectively, as revealed by XPS data. Core level XPS analysis of nitrogen of 0.5GN−AgBr depicts the amino, pyrrolic, and graphitic N, respectively, at 398.22, 399.71, and 401.33 eV, as shown in Figure 3B. It is worth noting that all the N binding energy values are smaller in 0.5GN−AgBr compared to the pure GN. It may be due to the interaction of the lone pair of electrons on N atoms in 0.5GN−AgBr with AgBr nanoparticles of the composite. Core level XPS spectra of C 1s in GO are also depicted in Figure S4A. The ratio of graphitic carbon to the carbon bonded oxygen atoms in GO, denoted as C/O, was calculated to be 0.44 and listed in Table S1.

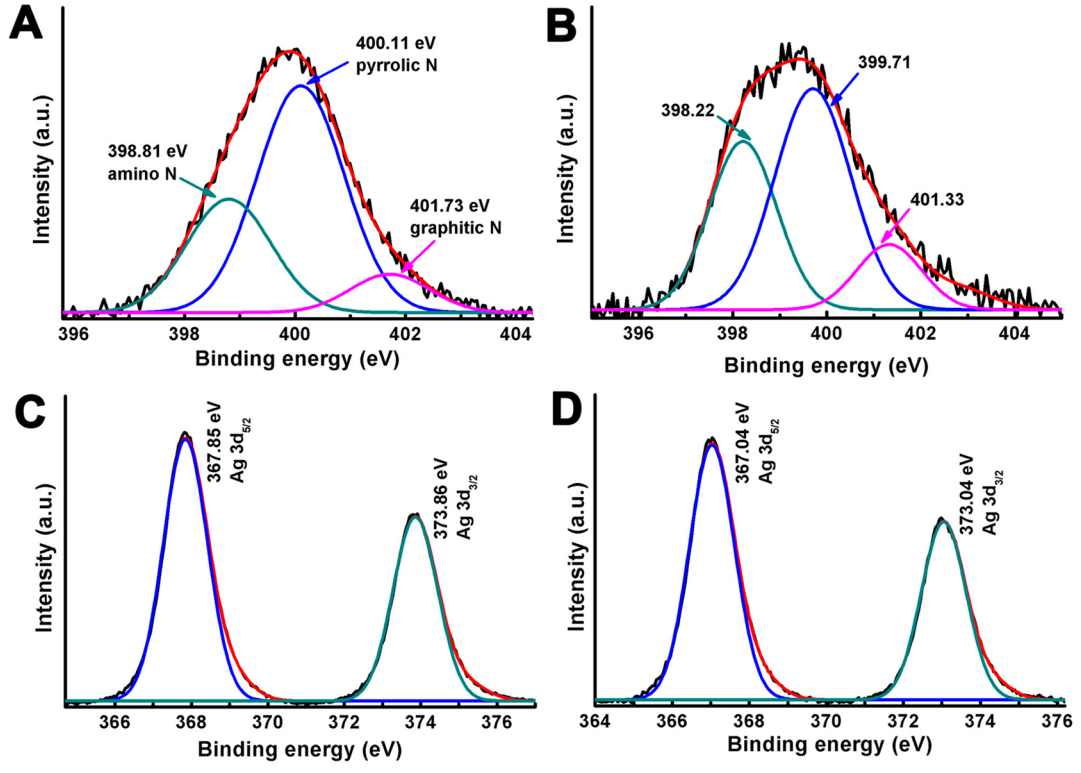

Figure 3. Core level X-ray photoelectron spectra of (A) N in GN, (B) N in 0.5GN−AgBr, (C) Ag in AgBr, and (D) Ag in 0.5GN−AgBr.

To elucidate the interactions, high resolution core level XPS spectra of Ag in AgBr and 0.5GN−AgBr were also investigated (Figure 3C and 3D). The discrete expression of doublet is assigned respectively to Ag $3d_{5/2}$ and Ag $3d_{3/2}$ of Ag^+ in AgBr.[47−50] While two peaks appeared at 367.85 and 373.86 eV for AgBr, these are shifted to 367.04 and 373.04 eV, respectively, in the 0.5GN−AgBr composite. A decrease in the binding energy with an amount of ∼0.8 eV might be attributed to the complexation of Ag^+ ions of the composite with the amine functionalized reduced graphene oxide through N-containing functionalities and COOH groups.[43] This characteristic was also identified in FTIR spectrum of 0.5GN−AgBr. High resolution XPS spectrum of Ag of the composite catalyst after 11 repeated cycles is depicted in Figure S4B. It revealed the presence of metallic Ag indicated by additional doublet formation at 368.43 and 373.53 eV, respectively, for Ag $3d_{5/2}$ and Ag $3d_{3/2}$. It points to the partial, yet fairly suppressed reduction of AgBr during the repeated photocatalytic experiments. The same conclusion was drawn from the XRD analysis of the composite catalyst after repeated uses. However, the C/O ratio of the catalyst of 0.5GN−AgBr has increased slightly, after 11 catalytic cycles, as shown in Table S1. It implies that the GN was reduced slightly during the 11 photocatalytic cycles. Table S1 also includes the concentration of N in the catalyst before experiment and after 11 catalytic cycles. It shows that concentration of N decreased slightly after 11 catalytic cycles, which may lead to the partial reduction of AgBr to metallic Ag as evidenced by XRD and XPS. The interaction of AgBr with O containing groups is not clear as evidenced from the core level XPS spectra of O 1s, which show nearly same binding energy values, in GN and 0.5GN−AgBr (see Figure S5 in Supporting Information). However, the interactions are likely to occur between Ag^+ of $AgNO_3$ and COO^- of GO because of the electrostatic attraction. The photocatalysts were analyzed for BET surface area, and the results are shown in Table S2. It shows that with increasing concentration of GN, specific surface area of the composites increases. Moreover, diffuse reflectance spectra (DRS) of the samples were measured, and results are shown in Figure S6. The band gap values are listed in Table S2. The DRS results show that absorption of the composites increases with increasing the amount of GN. All the composites have band gap placed in the visible region as evident from the spectra.

The photocatalytic activity and stability of the as prepared catalysts were evaluated by the photodegradation experiment of methylene blue dye under the visible light irradiation. All experiments were carried out for 50 min at ambient temperature (∼20 °C) and pressure. Prior to the dye degradation experiment, the mixture of the catalyst and dye was kept under stirring in the dark for 1 h. Figure S7 shows the concentration of the dye remaining in solution after reaching the equilibrium. It shows that the composites can adsorb more dye with increasing amounts of GN because of the increased surface area of the composites. As depicted in Figure 4A, only a little amount of MB was degraded after 50 min without photocatalysts, whereas ∼11% dye was degraded with GN, under the present experimental conditions. The as synthesized AgBr can degrade almost 50% of MB after the same time. In contrast, the catalytic activity of AgBr increases significantly when it forms nanocomposite with amine functionalized reduced graphene oxide. The result shows that almost 99% of MB was degraded with the catalysts of 0.5GN−AgBr and 1GN−AgBr after 50 min of photocatalytic experiment.

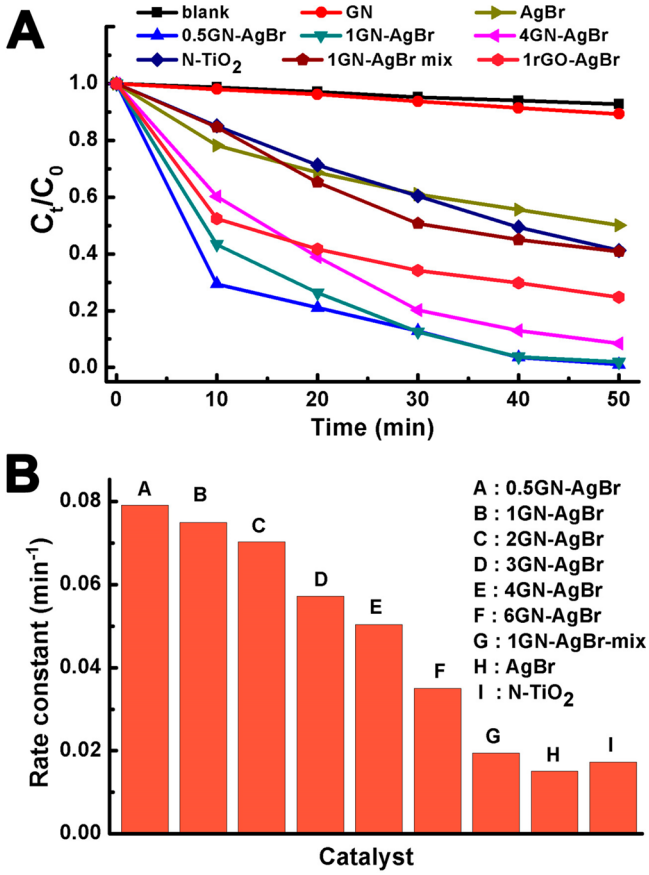

Figure 4. (A) Normalized concentration of dye solutions under degradation with different catalysts. (B) First order rate constants for the dye degradation experiments.

Increased amount of GN in the nanocomposites rather decreases catalytic activity (see Figures 4A and S8). It may be associated with an increase of the coverage of the active sites on the catalyst by the excess amount of GN. Moreover, as shown in Figure S6, the absorption of the photocatalysts increases with increasing amounts of GN in the composites. Although more light is absorbed with the catalysts with more GN, considerable amount of light is blocked by the presence of GN; thus, a reduced amount of light reaches the AgBr particles. This blocking effect of light also decreases the photocatalytic activity.

For comparisons, catalysts of 1GN−AgBr−mix, 1rGO−AgBr, and N−TiO_2 were also examined for their catalytic activity. As shown in Figure 4A, N−TiO_2 degrades ∼59% dye after 50 min of visible light irradiation, whereas 1GN−AgBr-mix can degrade ∼59% and 1rGO−AgBr degrades ∼75% of MB after the same time of photocatalytic experiment. The catalyst with the highest concentration of GN, 6GN−AgBr, merely degrades about 50% of MB (Figure S8) after 50 min under the same experimental conditions. Evolutional changes in UV−visible spectra of MB during the dye degradation experiment for the catalyst of 0.5GN−AgBr and the corresponding digital camera images are shown in Figures S9a and S9b, respectively. Catalytic performance was also measured with the catalyst 0.2GN−AgBr. It degrades ∼70% of MB after 50 min of experiment, as displayed in Figure S8.

The dye degradation reactions follow the first order kinetics. Figure 4B shows the first order rate constants of different catalysts. It shows that 0.5GN−AgBr has the highest rate

dx.doi.org/10.1021/am5051422 | ACS Appl. Mater. Interfaces 2014, 6, 20819−20827

constant (0.079 min^{-1}), followed by the catalyst 1GN−AgBr, which shows a rate constant of 0.078 min^{-1}. The rate constant of the catalyst 0.5GN−AgBr is 4.6, 5.3, and 4.0 times compared to N−TiO_2, AgBr, and 1GN−AgBr-mix, respectively. The first order rate constant decreases with increasing amounts of GN in the composites. Dye degradation efficiency also decreases with increasing amounts of GN in the catalysts.

To ensure the prolonged photocatalytic activity of the synthesized materials, 0.5GN−AgBr was used for recycled tests more than 10 times. Figure 5A shows the experimental results.

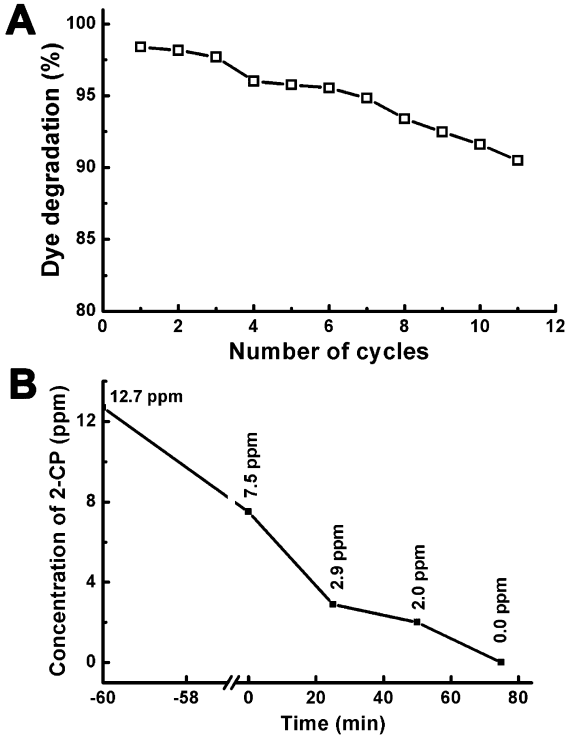

Figure 5. (A) Recyclability test of the catalyst 0.5GN−AgBr. It was recycled for 11 catalytic cycles. (B) Residual concentration of 2-chlorophenol (2-CP) at different times. It shows that 2-CP was degraded completely after 75 min of visible light irradiation in the presence of 0.5GN−AgBr.

It shows that ∼90% of MB was degraded even after 11 catalytic cycles, implying that the catalytic activity was fairly retained. The loss in catalytic activity may be due to the decrease in the N concentrations during the catalytic experiments as evidenced by XPS analysis. The efficiency of the catalyst was further tested to degrade organic phenolic compounds, e.g., 2-chlorophenol (2-CP), which is colorless and does not absorb in the visible region ($\lambda_{max} \approx 274$ nm). For this experiment, 30 mg of 0.5GN−AgBr was dispersed in 40 mL of 2-CP solution (12.6 ppm), and the mixture was kept stirring for 1 h in the dark. Figure 5B shows the concentration of 2-CP at different times. It shows that all the 2-CP was decomposed after 75 min of visible light exposure. To confirm a complete degradation of 2-CP, FTIR spectrum of the used catalyst was obtained (Figure S10a), in which no peak of 2-CP remained. Therefore, we can conclude that 2-CP was decomposed completely, not remained adsorbed over the catalyst. We further carried out experiments with more concentrated 2-CP solutions. The experimental result (Figure S10b) shows that ∼50% of 2-CP (60 ppm) was decomposed after 100 min. The degradation of 2-CP proves that the photodegradation of MB occurs as a result of the excitation of GN−AgBr, not because of the photoexcitation of MB.

Photocatalytic activity of the composites was further explored by measuring the photocurrent (Figure 6). The maximum

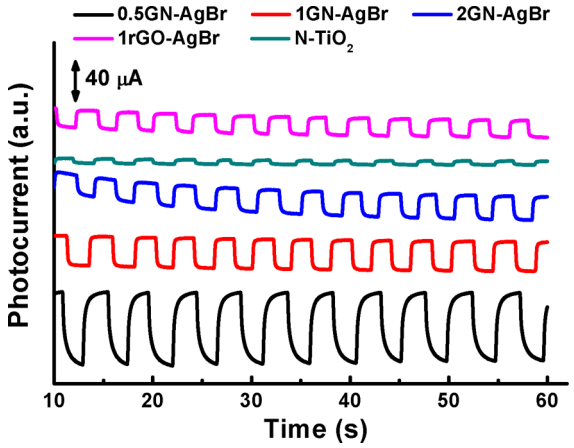

Figure 6. Photoelectrochemical measurement for different catalysts.

photocurrent was obtained with the catalyst 0.5GN−AgBr. The amount of photocurrent decreased with increasing amounts of GN in the composite. The results are consistent with the result of the degradation of MB. For comparison, the photocurrent data of rGO−AgBr and N−TiO_2 were also provided. It is clear from Figure 6 that the photocurrent of 1rGO−AgBr is weaker than the corresponding composite with GN, i.e., 1GN−AgBr. We believe that it can be attributed to the greater conductivity of GN compared to rGO due to the N-doping effect.

In many dye degradation reactions, hydroxyl radicals are generated as intermediate species. To analyze the ·OH radicals in our experiment, terephthalic acid was used as a probe molecule.[51] In a typical experiment, 30 mg of 0.5GN−AgBr was dispersed in 0.5 mM terephthalic acid in 2.0 mM aqueous solution of NaOH. The mixture was kept in the dark for 1 h under stirring condition. Then the reaction mixture was irradiated with visible light. Approximately 3 mL of the reaction mixture was collected with a regular time interval, and the catalyst was separated by centrifugation (11 000 rpm, 10 min). The supernatant was characterized by fluorescence spectrometer. Figure 7A shows zero fluorescence intensity at the beginning of the experiment. However, the fluorescent intensity increases with time and the peak position matches well with that of 2-hydroxyterephthalic acid. During the experiment, terephthalic acid, which is not fluorescent active, undergoes reaction with the ·OH radicals generated in the reaction mixture to give rise to 2-hydroxyterephthalic acid, which is a fluorescent (λ at ∼425 nm) active material.[51] The chemical reaction that occurs is shown in Scheme S1 in the Supporting Information. This experimental result proves that the catalyst generates OH radicals in the reaction medium.

To detect possible participation of other active species during photocatalytic reactions, superoxide radicals ($O_2^{-\bullet}$) and holes (h^+) were investigated. The photocatalytic experiments are similar to the one described earlier except 1 mM triethanolamine (TEA), a quencher of h^+ and *p*-benzoquinone (BQ), a quencher of $O_2^{-\bullet}$ were used in separate experiments. The experimental results are shown in Figure S11. It is clear from the figure that the photodegradation of MB was suppressed

dx.doi.org/10.1021/am5051422 | ACS Appl. Mater. Interfaces 2014, 6, 20819−20827

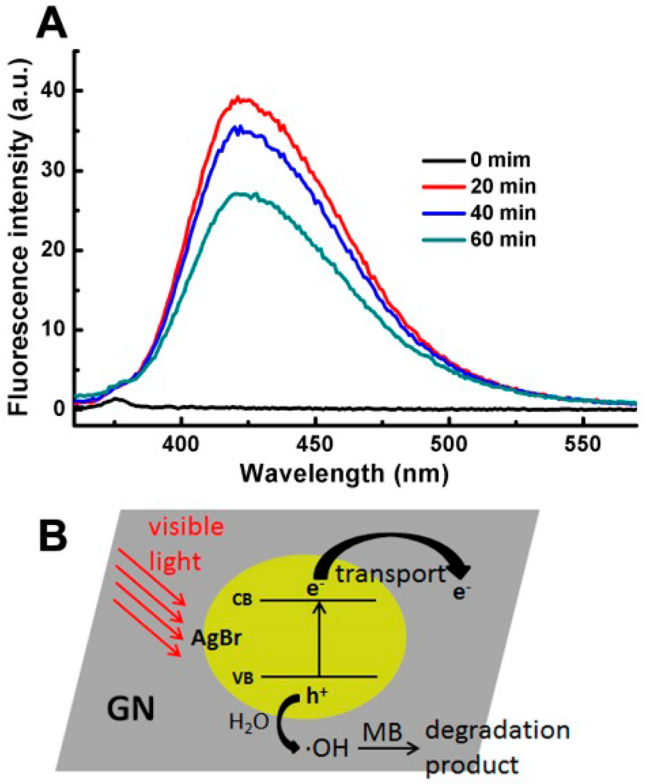

Figure 7. (A) Fluorescence intensity of the reaction mixture of 0.5 mM terephthalic acid in 2.0 mM NaOH in the presence of the catalyst 0.5GN−AgBr under the irradiation of visible light. (B) Schematic to show the degradation mechanism of MB under visible light.

after the addition of TEA and BQ. These results prove that h^+ and $O_2^{-\bullet}$ play an important role in the photodegradation process.

On the basis of the above-mentioned experimental results, a plausible mechanism is proposed for the high photocatalytic activity and stability of the nanocomposite photocatalyst systems and is shown in Figure 7B. The active catalyst, AgBr, can absorb visible light, and a large number of electron−hole pairs are generated. The conduction electrons are then transported to the GN. The excellent conductivity of GN can greatly increase the electron mobility, thus enhancing the interfacial charge transfer.[38,41] This will effectively reduce the undesired recombination of electron−hole pairs. The electrons may be adsorbed by dissolved oxygen and water molecules on the photocatalyst surface to generate O_2^-, $O_2^{-\bullet}$, and other reactive oxygen species, which are further combined with water to form OH radicals.[9,10] On the other hand, the holes in the valence band can directly oxidize water to form OH radicals.[9,10] The highly reactive hydroxyl radicals then degrade the dye molecules.

$$e^- + O_2 + H_2O \rightarrow \cdot OH$$

$$h^+ + H_2O \rightarrow \cdot OH$$

$$\cdot OH + MB \rightarrow \text{degradation product}$$

The proposed reactions are shown in the above equations. The holes, in the valence band, also can directly oxidize MB molecules. Another important factor in the dye degradation process is the adsorption of MB molecules on the photocatalyst. The π-electrons in GN can create $\pi-\pi$ interactions with MB molecules. Moreover, Ag^+ ions in AgBr can undergo complexation with the nitrogen and sulfur atoms in MB molecules. These two factors consequently promote the MB molecules to be in intimate contact with the photocatalyst and fast degradation of the dye. It must be pointed out here that the highly conducting GN can transfer conduction electrons far away from AgBr as soon as they are generated rather than being trapped by the Ag^+ ions in AgBr. Therefore, the Ag^+ ions in AgBr can circumvent the reduction reaction to the maximum extent; thus, only a minimal amount of metallic Ag was generated after prolonged use of the catalysts.[1] In this way, the catalytic activity was maintained and the stability of the catalyst was also ensured to a great extent.

CONCLUSIONS

Nanocomposites of AgBr with nitrogen doped and amine functionalized reduced graphene oxide (GN) were synthesized through a simple and environmentally benign reaction route. The nanocomposites, as compared to the as synthesized AgBr or nitrogen doped titania ($N-TiO_2$), exhibit enhanced photocatalytic activity toward the degradation of methylene blue dye. The best photocatalytic activity was observed with the catalyst having 0.5 wt % GN in the composite. It produces enhanced photocurrent compared to $N-TiO_2$. It is also observed that the nanocomposite of AgBr with GN is a better photocatalyst than the nanocomposite of rGO with AgBr-complexed ones for dye degradation and producing photocurrent. Since the optimal coverage of active sites on the photocatalyst surface is influenced by the amount of GN complexation, the observed catalytic activity decreases with increasing amounts of GN in the composites. In addition, the composite can remove 2-chlorophenol from contaminated water with a high efficiency. Notably, the catalyst can be recycled more than 10 times with minimal loss of photocatalytic activity. The generation of hydroxyl radicals plays an important role in the efficient dye degradation process.

ASSOCIATED CONTENT

Supporting Information

XRD, SEM, and XPS of the catalyst after 11 repeated cycles in Figures S1, S2, and S4B; Figure S3 showing the TEM of 2GN−AgBr; C 1s XPS spectrum of GO in Figure S4A; XPS of O 1S of GN and 0.5GN−AgBr in Figure S5a and Figure S5b; Figure S6 describing UV-DRS results; adsorption of MB by all the catalysts and degradation of MB by other catalysts in Figures S7 and S8, respectively; Figure S9a and Figure S9b respectively depicting real time UV−visible spectra and digital image of MB at different times; Figure S10a showing the FTIR spectra of 2-CP and the catalyst 0.5GN−AgBr before and after use; concentration of 2-CP at different times in Figure S10b; Scheme S1 describing the chemical reaction of terephthalic acid with ·OH radicals to give 2-hydroxyterephthalic acid; band gap and BET surface area of the catalysts in Table S2; Figure S11 describing the effect of different scavengers in the degradation of MB. This material is available free of charge via the Internet at http://pubs.acs.org.

AUTHOR INFORMATION

Corresponding Author

*E-mail: pjyoo@skku.edu.

Notes

The authors declare no competing financial interest.

■ ACKNOWLEDGMENTS

This work was supported by research grants of NRF (Grant 2012M1A2A2671795), Global Frontier R&D Program on Center for Multiscale Energy System (Grant 2012M3A6A7055540), and Basic Science Research Program (Grant 2010-0027955) funded by the National Research Foundation under the Ministry of Science, ICT & Future, Korea.

■ REFERENCES

(1) Kuai, L.; Geng, B.; Chen, X.; Zhao, Y.; Luo, Y. Facile Subsequently Light-Induced Route to Highly Efficient and Stable Sunlight-Driven Ag−AgBr Plasmonic Photocatalyst. *Langmuir* **2010**, *26*, 18723−18727.

(2) Xiong, W.; Zhao, Q.; Li, X.; Zhang, D. One-Step Synthesis of Flower-Like Ag/AgCl/BiOCl Composite with Enhanced Visible-light Photocatalytic Activity. *Catal. Comm.* **2011**, *16*, 229−233.

(3) Wu, M.; Jin, Y.; Zhao, G.; Li, M.; Li, D. Electrosorption-Promoted Photodegradation of Opaque Wastewater on a Novel TiO_2/Carbon Aerogel Electrode. *Environ. Sci. Technol.* **2010**, *44*, 1780−1785.

(4) Lin, D. D.; Wu, H.; Zhang, R.; Pan, W. Enhanced Photocatalysis of Electrospun Ag-ZnO Heterostructured Nanofibers. *Chem. Mater.* **2009**, *21*, 3479−3484.

(5) Fujihira, M.; Satoh, Y.; Osa, T. Heterogeneous Photocatalytic Oxidation of Aromatic Compounds on TiO_2. *Nature* **1981**, *293*, 206−208.

(6) Li, H. Y.; Wang, D. J.; Wang, P.; Fan, H. M.; Xie, T. F. Synthesis and Studies of the Visible-Light Photocatalytic Properties of Near-Monodisperse Bi-Doped TiO_2 Nanospheres. *Chem.—Eur. J.* **2009**, *15*, 12521−12527.

(7) Huang, J. H.; Cui, Y. J.; Wang, X. C. ZrO_2-Modified Mesoporous Nanocrystalline $TiO_{2-x}N_x$ as Efficient Visible Light Photocatalysts. *Environ. Sci. Technol.* **2010**, *44*, 3500−3504.

(8) Zeng, H. B.; Cai, W. P.; Liu, P. S.; Xu, X. X.; Zhou, H. J.; Klingshirn, C.; Kalt, H. ZnO-Based Hollow Nanoparticles by Selective Etching: Elimination and Reconstruction of Metal−Semiconductor Interface, Improvement of Blue Emission and Photocatalysis. *ACS Nano* **2008**, *2*, 1661−1670.

(9) Sher Shah, M. S. A.; Zhang, K.; Park, A. R.; Kim, K. S.; Park, N.-G.; Park, J. H.; Yoo, P. J. Single-step Solvothermal Synthesis of Mesoporous Ag−TiO_2−Reduced Graphene Oxide Ternary Composites with Enhanced Photocatalytic Activity. *Nanoscale* **2013**, *5*, 5093−5101.

(10) Sher Shah, M. S. A.; Park, A. R.; Zhang, K.; Park, J. H.; Yoo, P. J. Green Synthesis of Biphasic TiO_2-Reduced Graphene Oxide Nanocomposites with Highly Enhanced Photocatalytic Activity. *ACS Appl. Mater. Interfaces* **2012**, *4*, 3893−3901.

(11) Wang, P.; Huang, B.; Zhang, X.; Qin, X.; Jin, H.; Dai, Y.; Wang, Z.; Wei, J.; Zhan, J.; Wang, S.; Wang, J.; Whangbo, M.-H. Highly Efficient Visible-Light Plasmonic Photocatalyst Ag@AgBr. *Chem.—Eur. J.* **2009**, *15*, 1821−1824.

(12) Elahifard, M. R.; Rahimnejad, S.; Haghighi, S.; Gholami, M. R. Apatite-Coated Ag/AgBr/TiO_2 Visible-Light Photocatalyst for Destruction of Bacteria. *J. Am. Chem. Soc.* **2007**, *129*, 9552−9553.

(13) Zang, Y. J.; Farnood, R. Photocatalytic Activity of AgBr/TiO_2 in Water under Simulated Sunlight Irradiation. *Appl. Catal., B* **2008**, *79*, 334−340.

(14) Zang, Y. J.; Farnood, R.; Currie, J. Photocatalytic Activities of AgBr/Y-Zeolite in Water under Visible Light Irradiation. *Chem. Eng. Sci.* **2009**, *64*, 2881−2886.

(15) Zhu, M. S.; Chen, P. L.; Liu, M. H. Graphene Oxide Enwrapped Ag/AgX (X = Br, Cl) Nanocomposite as a Highly Efficient Visible-Light Plasmonic Photocatalyst. *ACS Nano* **2011**, *5*, 4529−4536.

(16) Wang, P.; Huang, B. B.; Qin, X. Y.; Zhang, X. Y.; Dai, Y.; Wei, J. Y.; Whangbo, M. H. Ag@AgCl: A Highly Efficient and Stable Photocatalyst Active under Visible Light. *Angew. Chem., Int. Ed.* **2008**, *47*, 7931−7933.

(17) Bi, Y. P.; Ye, J. H. Direct Conversion of Commercial Silver Foils into High Aspect Ratio AgBr Nanowires with Enhanced Photocatalytic Properties. *Chem.—Eur. J.* **2010**, *16*, 10327−10331.

(18) Grabowska, E.; Zaleska, A.; Sorgues, S.; Kunst, M.; Etcheberry, A.; Colbeau-Justin, C.; Remita, H. Modification of Titanium(IV) Dioxide with Small Silver Nanoparticles: Application in Photocatalysis. *J. Phys. Chem. C* **2013**, *117*, 1955−1962.

(19) Tao, A.; Kim, F.; Hess, C.; Goldberger, J.; He, R.; Sun, Y.; Xia, Y.; Yang, P. Langmuir−Blodgett Silver Nanowire Monolayers for Molecular Sensing Using Surface-Enhanced Raman Spectroscopy. *Nano Lett.* **2003**, *3*, 1229−1233.

(20) Chen, M. W.; Chau, Y. F.; Tsai, D. P. Three-Dimensional Analysis of Scattering Field Interactions and Surface Plasmon Resonance in Coupled Silver Nanospheres. *Plasmonics* **2008**, *3*, 157−162.

(21) Zhu, M.; Chen, P.; Ma, W.; Lei, B.; Liu, M. Template-Free Synthesis of Cube-like Ag/AgCl Nanostructures via a Direct-Precipitation Protocol: Highly Efficient Sunlight-Driven Plasmonic Photocatalysts. *ACS Appl. Mater. Interfaces* **2012**, *4*, 6386−6392.

(22) Zhu, M.; Chen, P.; Liu, M. Ag/AgBr/Graphene Oxide Nanocomposite Synthesized via Oil/Water and Water/Oil Microemulsions: A Comparison of Sunlight Energized Plasmonic Photocatalytic Activity. *Langmuir* **2012**, *28*, 3385−3390.

(23) Luo, G.; Jiang, X.; Li, M.; Shen, Q.; Zhang, L.; Yu, H. Facile Fabrication and Enhanced Photocatalytic Performance of Ag/AgCl/rGO Heterostructure Photocatalyst. *ACS Appl. Mater. Interfaces* **2013**, *5*, 2161−2168.

(24) Zhang, X. Y.; Li, H. P.; Cui, X. L.; Lin, Y. H. Graphene/TiO_2 Nanocomposites: Synthesis, Characterization and Application in Hydrogen Evolution from Water Photocatalytic Splitting. *J. Mater. Chem.* **2010**, *20*, 2801−2806.

(25) Lambert, T. N.; Chavez, C. A.; Hernandez-Sanchez, B. H.; Lu, P.; Bell, N. S.; Ambrosini, A.; Friedman, T.; Boyle, T. J.; Wheeler, D. R.; Huber, D. L. Synthesis and Characterization of Titania−Graphene Nanocomposites. *J. Phys. Chem. C* **2009**, *113*, 19812−19823.

(26) Dreyer, D. R.; Park, S.; Bielawski, C. W.; Ruoff, R. S. The Chemistry of Graphene Oxide. *Chem. Soc. Rev.* **2010**, *39*, 228−240.

(27) Zhang, N.; Zhang, Y.; Xu, Y.-J. Recent Progress on Graphene-Based Photocatalysts: Current Status and Future Perspectives. *Nanoscale* **2012**, *4*, 5792−5813.

(28) Yang, M.-Q.; Xu, Y.-J. Selective Photoredox Using Graphene-Based Composite Photocatalysts. *Phys. Chem. Chem. Phys.* **2013**, *15*, 19102−19118.

(29) Han, C.; Yang, M.-Q.; Weng, B.; Xu, Y.-J. Improving the Photocatalytic Activity and Anti-Photocorrosion of Semiconductor ZnO by Coupling with Versatile Carbon. *Phys. Chem. Chem. Phys.* **2014**, *16*, 16891−16903.

(30) Zhang, Y.; Tang, Z.-R.; Fu, X.; Xu, Y.-J. TiO_2−Graphene Nanocomposites for Gas-Phase Photocatalytic Degradation of Volatile Aromatic Pollutant: Is TiO_2−Graphene Truly Different from Other TiO_2−Carbon Composite Materials? *ACS Nano* **2010**, *4*, 7303−7314.

(31) Liu, S.; Yang, M.-Q.; Xu, Y.-J. Surface Charge Promotes the Synthesis of Large, Flat Structured Ggraphene−(CdS nanowire)−TiO_2 Nanocomposites as Versatile Visible Light Photocatalysts. *J. Mater. Chem. A* **2014**, *2*, 430−440.

(32) Zhang, N.; Zhang, Y.; Pan, X.; Yang, M.-Q.; Xu, Y.-J. Constructing Ternary CdS−Graphene−TiO_2 Hybrids on the Flatland of Graphene Oxide with Enhanced Visible-Light Photoactivity for Selective Transformation. *J. Phys. Chem. C* **2012**, *116*, 18023−18031.

(33) Zhang, Y.; Tang, Z.-R.; Fu, X.; Xu, Y.-J. Engineering the Unique 2D Mat of Graphene to Achieve Graphene-TiO_2 Nanocomposite for Photocatalytic Selective Transformation: What Advantage Does Graphene Have over Its Forebear Carbon Nanotube? *ACS Nano* **2011**, *5*, 7426−7435.

(34) Zhang, Y.; Zhang, N.; Tang, Z.-R.; Xu, Y.-J. Graphene Transforms Wide Band Gap ZnS to a Visible Light Photocatalyst. The New Role of Graphene as a Macromolecular Photosensitizer. *ACS Nano* **2012**, *6*, 9777−9789.

(35) Zhang, N.; Yang, M.-Q.; Tang, Z.-R.; Xu, Y.-J. Toward Improving the Graphene−Semiconductor Composite Photoactivity via the Addition of Metal Ions as Generic Interfacial Mediator. *ACS Nano* **2014**, *8*, 623−633.
(36) Yang, H.; Shan, C.; Li, F.; Han, D.; Zhang, Q.; Niu, L. Covalent Functionalization of Polydisperse Chemically-Converted Graphene-sheets with Amine-Terminated Ionic Liquid. *Chem. Commun.* **2009**, 3880−3882.
(37) Lherbier, A.; Blase, X.; Niquet, Y.-M.; Triozon, F.; Roche, S. Charge Transport in Chemically Doped 2D Graphene. *Phys. Rev. Lett.* **2008**, *101* (036808), 1−4.
(38) Zhang, C.; Hao, R.; Liao, H.; Hou, Y. Synthesis of Amino-Functionalized Graphene as Metal-Free Catalyst and Exploration of the Roles of Various Nitrogen States in Oxygen Reduction Reaction. *Nano Energy* **2013**, *2*, 88−97.
(39) Wang, Y.; Shao, Y.; Matson, D. W.; Li, J.; Lin, Y. Nitrogen-Doped Graphene and Its Application in Electrochemical Biosensing. *ACS Nano* **2010**, *4*, 1790−1798.
(40) Wang, X.; Li, X.; Zhang, L.; Yoon, Y.; Weber, P. K.; Wang, H.; Guo, J.; Dai, H. N-Doping of Graphene through Electrothermal Reactions with Ammonia. *Science* **2009**, *324*, 768−771.
(41) Lai, L.; Chen, L.; Zhan, D.; Sun, L.; Liu, J.; Lim, S. H.; Poh, C. K.; Shen, Z.; Lin, J. One-Step Synthesis of NH_2-Graphene from in Situ Graphene-Oxide Reduction and Its Improved Electrochemical Properties. *Carbon* **2011**, *49*, 3250−3257.
(42) Yuan, C.; Chen, W.; Yan, L. Amino-Grafted Graphene as a Stable and Metal-Free Solid Basic Catalyst. *J. Mater. Chem.* **2012**, *22*, 7456−7460.
(43) Xu, Y.-S.; Zhang, W.-D. Ag/AgBr-Grafted Graphite-like Carbon Nitride with Enhanced Plasmonic Photocatalytic Activity under Visible Light. *ChemCatChem* **2013**, *5*, 2343−2351.
(44) Yang, G.; Jiang, Z.; Shi, H.; Xiao, T.; Yan, Z. Preparation of Highly Visible-Light Active N-Doped TiO_2 Photocatalyst. *J. Mater. Chem.* **2010**, *20*, 5301−5309.
(45) Wang, J.; An, C.; Liu, J.; Xi, G.; Jiang, W.; Wang, S.; Zhang, Q.-H. Graphene Oxide Coupled AgBr Nanosheets: An Efficient Dual-Functional Visible-Light-Responsive Nanophotocatalyst with Enhanced Performance. *J. Mater. Chem. A* **2013**, *1*, 2827−2832.
(46) Sher Shah, M. S. A.; Nag, M.; Kalagara, T.; Singh, S.; Manorama, S. V. Silver on PEG-PU-TiO_2 Polymer Nanocomposite Films: An Excellent System for Antibacterial Applications. *Chem. Mater.* **2008**, *20*, 2455−2460.
(47) Wang, X.; Tang, Y.; Chen, Z.; Lim, T.-T. Highly Stable Heterostructured Ag−AgBr/TiO_2 Composite: A Bifunctional Visible-Light Active Photocatalyst for Destruction of Ibuprofen and Bacteria. *J. Mater. Chem.* **2012**, *22*, 23149−23158.
(48) Xu, H.; Xu, Y.; Li, H.; Xia, J.; Xiong, J.; Yin, S.; Huang, C.; Wan, H. Synthesis, Characterization and Photocatalytic Property of AgBr/$BiPO_4$ Heterojunction Photocatalyst. *Dalton Trans.* **2012**, *41*, 3387−3394.
(49) Xu, H.; Yan, J.; Xu, Y.; Song, Y.; Li, H.; Xia, J.; Huang, C.; Wan, H. Novel Visible-Light-Driven AgX/Graphite-Like C_3N_4 (X=Br, I) Hybrid Materials with Synergistic Photocatalytic Activity. *Appl. Catal., B* **2013**, *129*, 182−193.
(50) Chen, J.; Zhu, J.; Da, Z.; Xu, H.; Yan, J.; Ji, H.; Shu, H.; Li, H. Improving the Photocatalytic Activity and Stabilityof Graphene-like BN/AgBr Composites. *Appl. Surf. Sci.* **2014**, *313*, 1−9.
(51) Li, T. B.; Chen, G.; Zhou, C.; Shen, Z. Y.; Jin, R. C.; Sun, J. X. New Photocatalyst BiOCl/BiOI Composites with Highly Enhanced Visible Light Photocatalytic Performances. *Dalton Trans.* **2011**, *40*, 6751−6758.